Chemical Synthesis of Graphite Perfluorooctanesulfonate Using K_2MnF_6 in Hydrofluoric Acid or Mixed Acid Solutions

Xuerong Zhang and Michael M. Lerner*

Department of Chemistry and Center for Advanced Materials Research, Oregon State University, Corvallis, Oregon 97331-4003

Received November 11, 1998. Revised Manuscript Received February 18, 1999

Graphite intercalation compounds (GICs) of nominal composition $C_xC_8F_{17}SO_3 \cdot yF$ are prepared under ambient conditions in 48% hydrofluoric acid, using the oxidant K_2MnF_6. The product compositions are evaluated by mass uptake, TGA, DSC, and elemental analysis. PXRD analysis indicates that the stable product after 3−4 day reaction ($x \cong 18$, $y \cong 4$) is a GIC comprised of a solid solution of stage 2 and stage 3. A similar product, although containing a greater graphite fluoride impurity, can be obtained within 1 h using this method at 50 °C. Longer reactions at elevated temperature lead to product degradation and other impurities. The addition of up to 83 vol % concentrated HNO_3 or 17% fuming H_2SO_4 produces a stage 2 intercalation compound within hours. One-dimensional structural modeling for the stage 2 GIC provides refined values for the graphene carbon/intercalant mole ratio, distance between graphene and sulfonate oxygen planes, position of additional intercalated fluoride, and the chain takeoff angle. The products obtained by this synthetic method and the observed staging phenomena are related to previous reports on graphite fluorometalates and an energetic model for graphite intercalation.

Introduction

Graphite is the only layered structure to undergo an extensive intercalation chemistry by both oxidative and reductive processes. Graphite intercalation compounds (GICs) are also unusual in the common occurrence of several well-defined stages, i.e., phases with ordered arrangements of occupied and unoccupied galleries. The Daumas−Herold domain model has been widely used to describe this staging phenomenon.[1] A schematic representation of a stage 2 GIC in Figure 1, with alternating galleries occupied by intercalant, indicates the relationship between the basal repeat length (I_c), gallery height (d_i), and stage (n). The integral stage number indicates the number of galleries contained in a repeat sequence where only the first is occupied by intercalant. The relationship between these parameters can also be expressed as

$$I_c = d_i + (n - 1)\,(3.354\ \text{Å}) \qquad (1)$$

According to this model, fractional stages can also be envisioned, for example stage 3/2 would refer to an occupancy between stage 1 and 2, where the repeat sequence contains 3 galleries, with the first two galleries being occupied.

The combination of extensive staging and broad intercalant chemistry allows a wide range of graphite intercalation reactions and compounds.[2−4] In addition to the basic research interest in GICs and associated chemistry, some of these materials have electrochemical properties that have become important in charge storage devices.[5−7] GICs are also important as precursors to malleable graphite forms.[8] New practical and scalable synthetic methods need to be developed to expand these applications.

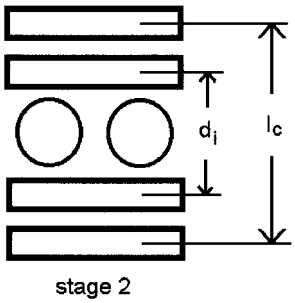

Figure 1. Representation for a stage 2 GIC showing relation of d_i and I_c.

Boehm and co-workers first described the intercalation of perfluoroalkylsulfonate anions into graphite, they prepared these compounds by the electrochemical oxidation of graphite in the corresponding acids at elevated

(1) Daumas, N.; Herold, A. *C. R. Acad. Sci.* **1969**, *C268*, 373.
(2) Bartlett, N.; McQuillan, B. In *Intercalation Chemistry*; Whittingham, S., Jacobson, A., Eds.; Academic Press: New York, 1982.
(3) Zabel, H., Solin, S. Eds. *Graphite Intercalation Compounds I*; Springer-Verlag: Berlin, 1990.
(4) Watanabe, N.; Touhara, H.; Nakajima, T.; Bartlett, N.; Mallouk, T.; Selig, H. In *Inorganic Solid Fluorides*; Hagenmuller, P., Ed.; Academic Press: New York, 1985.
(5) Guerard, D.; Herold, A. *Carbon* **1975**, *13*, 337.
(6) Ozawa, K. *Solid State Ionics* **1994**, *69*, 212.
(7) Markovsky, B.; Levi, M.; Aurbach, D. *Electrochim. Acta* **1998**, *43*, 2287.
(8) Buckley, J., Edie, D., Eds. *Carbon−carbon materials and composites*; Noyes Publ.: NJ, 1993.

10.1021/cm981060v CCC: $18.00
Published on Web 03/27/1999

temperature.[9] These studies include the significant observation that GICs were formed with greatly expanded galleries when $n > 4$ in $C_nF_{2n+1}SO_3^-$. The distance between graphene carbon planes encasing intercalated galleries, d_i, was found to be ~34 Å for the perfluorooctanesulfonate compound, $C_xC_8F_{17}SO_3$ or C_xPFOS, which strongly suggested a bilayer intercalant structure. The bilayer arrangement is a common intercalant orientation upon exchange of smectite clays[10] or for other layered metal oxides or sulfides when intercalated with surfactant-like cations.[11] This bilayer arrangement is favorable as it allows increased interaction between the charged sheet surface and oppositely charged headgroups, and also close interaction between nonpolar chains at the gallery centers. These reports demonstrated for the first time that graphite could form intercalation compounds with galleries larger than 10 Å and provided the first example of an amphoteric bilayer intercalant structure in a GIC.

In 1996, our group reported a study on C_xPFOS where the target compounds were prepared by the electrochemical oxidation of graphite in $LiC_8F_{17}SO_3$ (sat.)/CH_3NO_2 at ambient temperature.[12] Compounds of stages 2−7 were obtained, with $d_i \cong 25-6$ Å for all the stages, and $x \cong 17$ for the stage 2 product.

In both the above studies, the electrosynthetic reactions are inherently limited by the low charge density required to avoid a large overpotential at the carbon surface, which would result in electrolyte decomposition and passivation of the graphite surface. In addition, the high potential required for graphite oxidation limits the selection of binders, electrolytes, and current collectors. For these reasons, scalable electrochemical reactions are unlikely to be realized, and it is preferable to find chemical routes for the bulk preparation of such GICs.

In 1993, our group reported on the use of transition metal fluorosalts as oxidants in the formation of graphite bifluoride and planar sheet graphite fluorides:[13]

$$C_x \xrightarrow[\text{RT}]{\text{AMFn}\atop\text{anhyd HF}} C_xHF_2\cdot\delta HF\ (x > 28) \text{ or } C_xF\ (x > 2) \qquad (2)$$

$$M = \text{Mn(IV), Ni(IV), Co(III), or Fe(III)}$$

The extent of fluorination was found to be limited by the oxidizing power of the fluoroanion. In particular, Mn(IV), in the form of MnF_6^{2-}, was suitable for obtaining C_xF compounds with $x > 5$. A method similar to reaction 2, with the addition of a soluble perfluoroalkanesulfonate and oxidant to the anhydrous solution, could lead to intercalation of these anions, but the necessity of handling anhydrous HF may also tend to limit the practical application of such a method.

In earlier experiments with the oxidant MnF_6^{2-}, reaction 2 was also evaluated using aqueous hydrofluoric acid, allowing a simplified synthetic apparatus and procedure.[14] Although K_2MnF_6 is very stable in this solvent, no GIC products were recovered. The desired reaction sequence appears to be subverted by the instability of the graphite bifluoride salt intermediate in hydrofluoric acid. Thus, rather than the desired GIC, a disordered graphite is obtained. The relative stability of C_xPFOS, however, suggested that this might be successfully prepared in aqueous acid.

In this report, we describe chemical methods to produce C_xPFOS, using a simple and rapid benchtop procedure. In addition, we extend the characterization of this GIC by PXRD, elemental, and thermal analyses.

Experimental Section

Fuming H_2SO_4 (Baker, fuming 30−33 oleum %), concentrated HNO_3 (Mallinckrodt, 69.2%), and hydrofluoric acid (Mallinckrodt AR, 48% (w/o)) were used as received. $C_8F_{17}SO_2F$ (3M, experimental product) was treated with excess 20% KOH solution and refluxed at 120 °C overnight. The white precipitate $KC_8F_{17}SO_3$ was washed with distilled water and dried under vacuum at room temperature. Bright yellow K_2MnF_6 powder was synthesized according to a literature method by reduction of $KMnO_4$ (EM Science GR) using H_2O_2 (Mallinckrodt AR, 30% in aqueous solution) in a KF/hydrofluoric acid solution.[15] Two types of graphite reagent were used: SP-1 powder (Union Carbide, 100 μm average particle diameter) and natural graphite flakes (Aldrich, 1−2 μm).

In a typical reaction, the graphite powder (50.0 mg, 4.16 mmol) was added to a stirred hydrofluoric acid solution (15 mL) containing K_2MnF_6 (200 mg, 0.8 mmol) and $KC_8F_{17}SO_3$ (200 mg, 0.4 mmol) in a polyethylene flask. The reactions proceeded in air, in a fumehood, at the specified temperatures and times. *Caution—heating hydrofluoric acid produces hazardous vapors and must be carried out under controlled conditions in a fumehood.* Products were filtered and washed briefly with cold hydrofluoric acid, then briefly rinsed with hexane, and dried overnight at 25 °C and a pressure of less than 0.1 Torr. The mass uptake for the solid product was obtained after the final drying step.

In some experiments, graphite powders were oxidized in mixed acid solutions, H_2SO_4/HF or HNO_3/HF. *Caution—Hydrofluoric acid was cooled in an ice bath before the addition of the concentrated acids.* The ratios of acids were varied as indicated in the text. Other synthetic steps were as above.

PXRD data were collected on a Siemens D5000 powder diffractometer, using Cu Kα radiation, with 0.02-deg 2θ steps, between 1.5° and 60°. Collection times varied from 0.1 s/step for routine analyses to 1.0 s/step for data used in structural modeling. Thermal analyses of powdered samples were carried out at 5 °C/min using a Shimadzu TGA-50 and DSC-50Q. The carrier gas for the thermal analyses was purified N_2 (<5 ppm O_2) at 25 mL/min, however, the O_2 content of the gas is likely to be significantly higher due to outgassing from the instrument. Elemental analyses (C,H,N,S, and F) were performed by Desert Analytics (Tuscon, AZ).

Integration of ^{19}F NMR peaks for $-CF_3$ endgroups indicated that the $C_8F_{17}SO_2F$ reagent used contained 70% linear and 30% branched isomers, with the predominant branched isomer being $(CF_3)_2C(F)C_5F_{10}SO_2F$. The same isomeric composition of the potassium salt and prepared GIC's were assumed. Energy-minimized structural models for these anions were calculated by the Spartan program (4.1.1), using the semiempirical AM-1 method.

PXRD peak widths were analyzed according to the Williamson−Hall relation for strain and domain size:[16]

$$\text{fwhm} \times \cos\theta = (4 \sin\theta)(\xi/2) + (\lambda/t) \qquad (3)$$

where fwhm is the peak full width (in radians) at half-maximum, ξ is related to the lattice strain distribution, $\lambda = 1.5418$ Å, and t is the coherent domain size.

(9) Boehm, H.; Helle, W.; Ruisinger, B. *Synth. Met.* **1988**, *23*, 395.
(10) Pinnavaia, T. *Science* **1983**, *220*, 365.
(11) Jacobson, A. In *Intercalation Chemistry*; Whittingham, S., Jacobsen, A., Eds.; Academic Press: New York, 1982.
(12) Zhang, Z.; Lerner, M. *Chem. Mater.* **1996**, *8*, 257.
(13) Lemmon, J.; Lerner, M. *Carbon* **1993**, *31*, 437.
(14) Lemmon, J.; Lerner, M. ACS National Meeting, San Diego, March, 1994.
(15) Bode, H.; Jenssen, H.; Bandte, F. *Angew. Chem.* **1953**, *65*, 304.
(16) Williamson, G.; Hall, W. *Acta Metall.* **1953**, *1*, 22.

One-dimensional electron density maps were generated for centrosymmetric stage 2 cells using either the experimental diffraction data or a proposed structural model. Observed intensity data were used to generate structure factors after correction by a Lorentz-polarization (L_p) factor:

$$F_{obs}(00l) = \pm(I/L_p)^{1/2} \quad (4)$$

$$L_p = (1 + \cos^2 2\theta)/(\sin^2 \theta \cos \theta) \quad (5)$$

where I is the integrated peak intensity. The calculated structure factors were obtained using:

$$F_{calc}(00l) = \sum f_i \cos(2\pi l z_i) \quad (6)$$

where l is the Miller index, z_i the fractional c-axis coordinate of each atom, and f_i the angle-dependent scattering factor obtained from the literature.[17] Electron density maps were then generated for $z = 0-1$, at increments of 0.004, using the following relation:

$$\rho(z) = (1/c)\,[F_0 + \sum_{l=1}^{\infty} F_{00l} \cos(2\pi l z)] \quad (7)$$

where c is the cell dimension, and F_0 the zeroth-order structure factor. Data collected between 14 and 17.5° 2θ were excluded due to small, broad peaks at 5.8 and 5.4 Å, ascribed to a C_xF impurity phase. Structures were refined by minimizing the crystallographic R factor:

$$R = \sum |k|F_{obs}(00l)| - |F_{cal}(00l)||/\sum k|F_{obs}(00l)| \quad (8)$$

A powder X-ray diffraction pattern was simulated by the DIFFaX program (v1.76) for the proposed model, and compared with the observed PXRD. The DIFFaX software allows the introduction of probability in the stacking sequence in structural models.[18]

Results and Discussion

Products from Hydrofluoric Acid. When graphite is added to the solution of K_2MnF_6 and $KC_8F_{17}SO_3$ in hydrofluoric acid, the structure evolves rapidly through a series of stages or mixtures of stages of a graphite compound containing $C_8F_{17}SO_3$ (C_xPFOS). A relatively constant pattern is obtained after 15−24 h (Figure 2), although a broad peak around 40° appears at very long reaction times due to the precipitation of an amorphous Mn-containing phase. With the smaller particle natural graphite (1−2 μm), a similar final diffraction pattern is obtained after a 4-h reaction. After drying, the low-stage products no longer exhibit a metallic luster, as in graphite, and are instead observed to be hydrophobic, electrostatic powders.

Generally, PXRD patterns taken using the flat diffractometer sample orientation show strong preferred orientation of these platy particles, and most or all of the observed peaks are (00l) reflections. The PXRD patterns obtained are similar in general appearance to those previously reported by electrochemical oxidation of graphite in electrolytes containing the $C_8F_{17}SO_3^-$ anion, and at first most reflections appear to relate to an $I_c \cong 33-36$ Å, with a notable set of five strong peaks centered at $d \cong 3.4$ Å.

(17) Su, Z.; Coppens, P. *Acta Crystallogr.* **1997**, *A53*, 749.
(18) Treacy, M. M.; Newsam, J. M.; Deem, M. W. *Proc. R. Soc. London A* **1991**, *433*, 499.

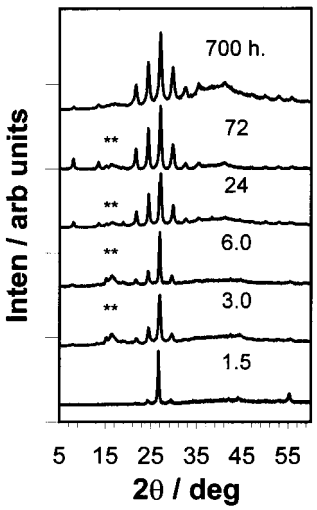

Figure 2. PXRD obtained at various reaction times for C_x-PFOS obtained by reaction of SP-1 graphite with a solution of $KC_8F_{17}SO_3$ and K_2MnF_6 in 48% hydrofluoric acid at 20 °C. The starred reflections at ~5.8 and 5.5 Å are ascribed to a C_xF impurity.

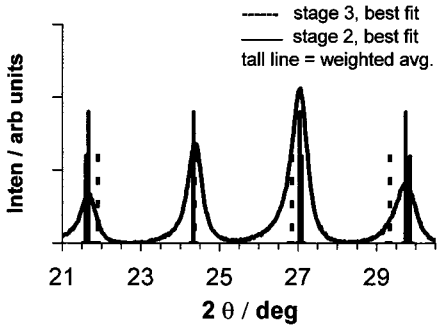

Figure 3. Calculated diffraction peak positions for stage 2, stage 3, and the 0.7:0.3 weighted average. The PXRD pattern overlay is that observed for the product after 72-h reaction using hydrofluoric acid.

Table 1. Peak Position Fits for Stage 2 and Stage 3 C_xPFOS, and a Weighted Average[a]

	stage 2		stage 3		stage 2/3
d obs, Å	index	d calc, Å	index	d calc, Å	d calc, Å
4.105	(008)	4.115	(009)	4.058	4.103
3.653	(009)	3.658	(0010)	3.653	3.657
3.299	(0010)	3.292	(0011)	3.321	3.298
3.005	(0011)	2.993	(0012)	3.044	3.004
RMS dev		0.018		0.064	0.005
I_c calc		32.921		36.526	32.971

[a] This solid product was prepared after 72-h reaction in hydrofluoric acid. The calculated root-mean-square deviations and lattice parameters are given for each case.

For the majority of XRD patterns obtained where hydrofluoric acid is used as a solvent, however, a reasonable fit of positions for these strong peaks found between 20° and 30° 2θ cannot be obtained using a single indexing cell parameter. In Figure 3 and Table 1, comparisons of best-fit data for a representative pattern are provided. As can be seen, the calculated peak positions using indices (008) − (0011) (I_c = 32.92 Å) are too far separated, and those using (009) − (0012) (I_c = 36.53 Å) are too close together. The assignment of these I_c values to stages 2 and 3 will be described later.

In these patterns, a better fit to the observed peak positions can be obtained using a weighted average of

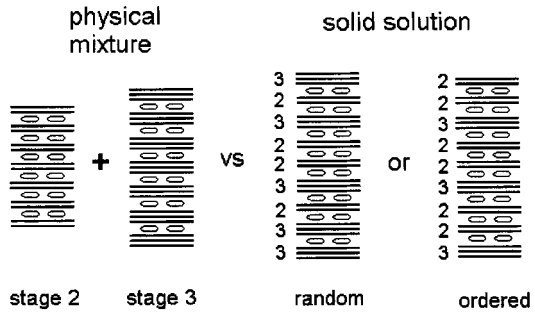

Figure 4. Schematic representations of GICs containing of a physical mixture of stage 2 and 3, and random or ordered solid solutions of second and third staging.

the stage 2 and 3 predicted positions. The stages in this fit are constrained to have the same values of d_i, such that I_c differs by exactly 3.354 Å for the two stages. Although a slight improvement in the fit can be obtained by allowing the gallery heights to differ, GICs are known to show similar gallery compositions and dimensions for stages >1. In the example given, the best fit was obtained using the combination of 79 mol % stage 2 and 21 mol % stage 3.

Two different structural models can be used to interpret these peak position data. The product may be modeled as containing either (1) a physical mixture of these stages, with overlapping peaks contributing to an averaged position, or (2) a solid solution of second and third staging, viz. a structure where either two or three graphene layers may separate the intercalated galleries. In the latter case, the staging sequence may exhibit some degree of ordering for the two or three graphene layers between galleries, or be entirely random. These different models are depicted in Figure 4.

In a physical mixture, the calculated weighting factor is approximately the relative abundance of each stage. In the solid solution model, the fractions of second staging and third staging content derived from peak positions will indicate the probability of either two or three graphene layers, respectively, between occupied galleries in the product. An assumption made in either case is that the overlapping peaks from the different stages have similar intensities. This is only approximately true, but the actual calculated peak intensities from this structural model, described below, can provide a more accurate composition.

Since $d = c/l$ for (00l) Bragg reflections of a given stage, the stage ($n + 1$) phase with the same value of d_i will generate reflections at

$$d\ (00l) = (c + 3.354\ \text{Å})/l \qquad (9)$$

The overlap of reflections from these phases can be described by the minimum separation, Δ, between calculated peak positions for the two patterns. This function has minima at $d = 3.35$ and 1.68 Å in the diffraction region investigated (see Figure 5), corresponding in the calculated example to the overlap of stage 2 (0,0,l) reflections with stage 3 (0,0,$l + 1$) reflections, and the overlap of stage 2 (0,0,l) with stage 3 (0,0,$l + 2$) reflections, respectively. The calculated peak separations at 5−15° 2θ indicate that the reflections from a physical mixture should be clearly resolvable, with peaks separated 1−2° 2θ. In each pattern obtained, however, only single reflections occur at low

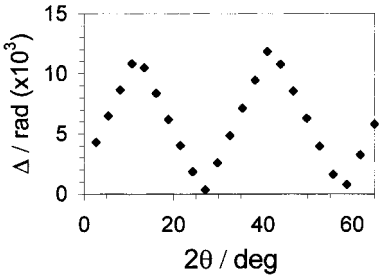

Figure 5. Plot of the minimum separation of peak positions (in radians), Δ, vs 2θ, where Δ is calculated for diffraction peaks of stage 2 and 3 GICs with $d_i = 33$ Å. The minima near 4 sin $\theta = 1$ and 2 arise from the overlap of stage 2 (0,0,l) with stage 3 (0,0,$l + 1$), and stage 2 (0,0,l) with stage 3 (0,0,$l + 2$), respectively.

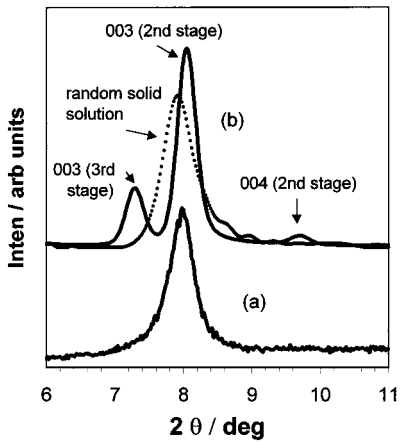

Figure 6. PXRD profiles (a) observed for C_xPFOS after reaction for 72 h in hydrofluoric acid, and (b) calculated for mixed phase and solid solution models. The solid line in b is for a physical mixture of stage 2 (70%) and stage 3 (30%), and the dotted line is for a random solid solution with those staging mole percents.

angle (Figure 6), indicating that these patterns do not arise from physical mixtures of the stages. These results, in combination with evidence from peak broadening (described below), indicate that these products are solid solutions containing second and third staging.

Two separate effects may be considered for contributing to peak broadening in solid solutions of stacking arrangements: (1) a Williamson−Hall broadening that relates increasing peak width to the finite coherent domain size and lattice strain in the stacking direction, and (2) a broadening due to the disordered presence of the two-component sequences (in this case, stage 2 and stage 3). It is expected that each of these may contribute to the overall fwhm for each reflection. The first effect will generate symmetric peak profiles with fwhm increasing as 4 sin θ. The second effect was here evaluated by generating recursive structural models for solid solutions containing second and third staging, and examining peak profiles obtained from the calculated patterns. The broadening calculated for the disordered solution has a similar periodic variation to the function Δ defined above, with minima at $d = 3.35$ and 1.68 Å, but is of lesser magnitude and generates asymmetric profiles for some peaks.

A Williamson−Hall plot (Figure 7) for the C_xPFOS product obtained following 72-h reaction in hydrofluoric acid shows that peak broadening does not follow the

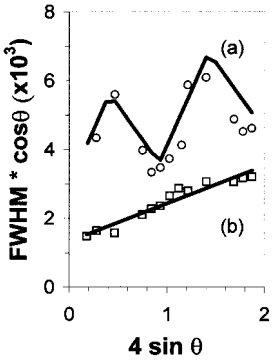

Figure 7. Williamson−Hall plots for two C_xPFOS products. In a, PXRD data (open circles) and the calculated trend (see text) are for a solid solution obtained from hydrofluoric acid. In b, PXRD data (open squares) and a best-fit line are for a product from hydrofluoric acid/nitric acid (17:83 v/v). Fwhm is the full width at half-peak maximum expressed in radians.

simple linear trend from the domain−strain effect. The peak widths obtained clearly show the periodic variation expected for a solid solution. The experimental values are seen to conform well to a fit using a combination of both broadening effects, a periodic variation overlying a linear increase due to a domain−strain effect, and the fit for this product is obtained using a random sequencing of second and third staging with a coherent domain size of ∼1000 Å. In marked contrast, the product obtained from a mixed acid solution (preparation described below), which is satisfactorily indexed as a simple stage 2 GIC, shows a good fit to the Williamson−Hall relation. The peak broadening data thus support a random solid solution model for the products obtained from hydrofluoric acid. Although degree of short-range ordering in the stacking direction might occur for each domain, the fit obtained using a completely random stacking sequence is not significantly improved by allowing such ordering.

After each reaction time studied, the products are best-fit as a solid solution containing a random combination of second and third staging. Using the fitting method described above for peak positions, the fractional mole content for each staging component is obtained, and these, along with the calculated d_i values and mass uptakes, are plotted against reaction time. (Figure 8) As can be seen, at 20 °C the second staging content increases to a maximum of 80% after approximately 100 h. No subsequent increase in the second staging content occurs even after reaction for 4 weeks, although the product obtained continues to increase in mass.

At 50 °C, the rate of intercalation increases significantly. The maximum intercalant content arises at ∼1−10 h, and PXRD patterns and mass uptakes for this product are similar to those at 20 °C. After 170-h reaction at 50 °C, a decrease in both the second staging content and the product mass indicate a loss of intercalant. At 70 °C, similar results are obtained, again with no evidence for the formation of a simple stage 2 C_x-PFOS.

The loss of intercalant at long reaction times and higher temperatures is related to the instability of the oxidant in hydrofluoric acid at these temperatures. The solution gradually loses the bright yellow color associated with MnF_6^{2-} after the maximum intercalant content is obtained, and an amorphous solid residue containing Mn, is produced. Although C_xPFOS is very stable in air over this time period,[19] this is not true in either liquid water or hydrofluoric acid. The air stability most likely originates from the formation of hydrophobic particle surfaces by $C_8F_{17}SO_3$, which can form a low surface energy monolayer and shield the positive graphite sheets effectively from water vapor in air. AFM studies have shown such an organized structure of PFOS forming at a graphite−solution interface.[20] In neat aqueous HF, however, the transition from stage 3 to a high stage will take place within several hours. When K_2MnF_6 is added to hydrofluoric acid, C_xPFOS is stabilized by reoxidation and will remain unchanged while the oxidant is present in solution. The decomposition of K_2MnF_6 at elevated temperature will therefore allow GIC reduction to proceed.

All the PXRD patterns show additional reflections at 5.8 and 5.5 Å, which occur in the region typical of (001) reflections from layered graphite fluorides. The relation of peak position in this region to composition has been evaluated previously.[21,22] The peak at 5.8 Å can be identified with an approximate composition of C_3F. The peak close to 5.5 Å overlaps with (006) from the C_xPFOS phase, but should correspond to a planar-sheet graphite fluoride, C_xF, $x \cong 4$. Products obtained using natural graphite (1 μm particle diameter) have greater intensities for these peaks than those derived from SP-1 graphite (100 μm particle diameter), suggesting that the side products arise at the particle edges. At 20 °C these impurity peaks are somewhat variable in intensity, but are often only a few percent of the total diffracted intensity. At a reaction temperature of 70 °C these peaks become similar in intensity to the strong peaks for C_xPFOS between 20° and 30° 2θ. (Figure 9).

The use of aqueous media for graphite intercalation is clearly restricted to acidic solutions due to the high potential required for graphite oxidation. Concentrated acids, such as fuming H_2SO_4 and 97% HNO_3, have long been used to prepare GICs of their conjugate anions.[2−4,23] By using the Nernst relation for the dependence of the water oxidation on activities of water and hydronium ion, an approximate relation for thermodynamic potential for oxidation of water in concentrated acid is

$$E \cong 1.23\ \text{V} - (0.059\ \text{V}) \log H_0 \qquad (10)$$

where H_0 represents the Hammett acidity function for a given acid solution. Figure 10 illustrates these derived potentials in relation to the potential ranges for various stages of C_xAsF_6. The potential ranges for stage formation are derived from the quasi equilibrium galvanostatic oxidation of graphite in anhydrous HF.[24] These potential-stage relations are well-defined for that system, but should be considered only as representative values here because the potentials depend to some extent on the nature of the intercalating anion. Still, it

(19) C_xPFOS shows 94% phase retention after 16 days in humid air. The exceptional air stability of this GIC will be reported separately.
(20) Lamont, R.; Ducker, W. *J. Colloid Interface Sci.* **1997**, *191*, 303.
(21) Mallouk, T.; Bartlett, N. *J. Chem. Soc., Chem. Commun.* **1983**, 103.
(22) Hagiwara, R.; Lerner, M.; Bartlett, N. *J. Chem. Soc., Chem. Commun.* **1989**, 573.
(23) Ubbelohde, A. *Proc. R. Soc. London A* **1968**, *304*, 25.
(24) Lerner, M. Ph.D. Thesis, UC Berkeley, 1988.

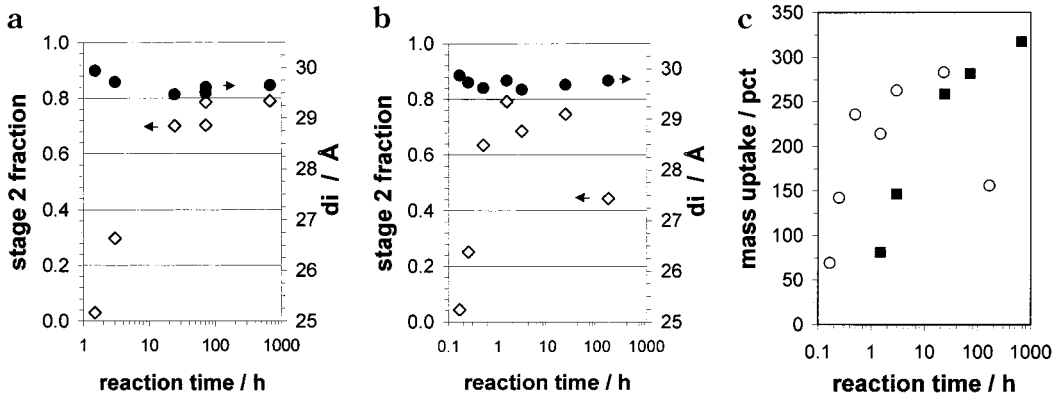

Figure 8. Second staging content (remainder is third staging) and d_i calculated from PXRD peak positions at various reaction times: (a) at 20 °C, and (b) at 50 °C. Mass uptakes for these products (■ = 20 °C, ○ = 50 °) are shown in c.

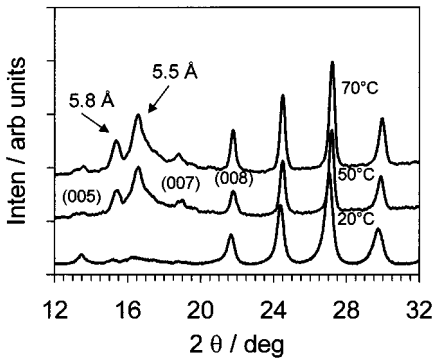

Figure 9. PXRD patterns for solid products obtained in hydrofluoric acid at 20, 50, and 70 °C. Reaction times are 24 h at 20 °C, and 15−30 min at 50 ° and 70 °C.

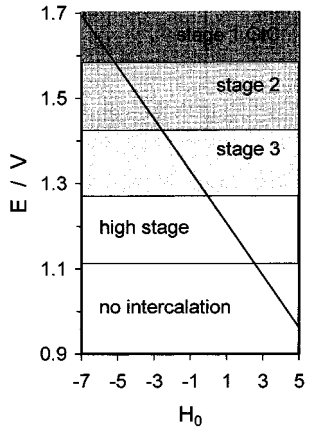

Figure 10. Approximate potential ranges for GIC stages. The solid line indicates the oxidation potential of water vs H_0.

is reasonable to suggest from this relation that 48% HF ($H_0 \cong -3.4$)[25] is sufficiently stable toward oxidation to allow formation of stage 2 or higher GICs.

The solid solution of stage 2 and 3 GIC described above is an example of a stable stage disorder, for it represents a product obtained at long reaction time without rearrangement to a simple integral stage or mixture of stages. Evidence for GICs with highly ordered fractional stages is not common, but there have been such observations for the donor-type GIC C_xK. A highly ordered stage 4/3 (that is, a repeat sequence of three intercalated then one empty gallery) was obtained by electrochemical reduction in THF,[26] and the existence of a 3/2 fractional stage at high pressure was confirmed by PXRD.[27] In these cases, the chemical potential energy of the fractional stages must be sufficiently different to permit the stabilization relative to an integral stage. There are several reports, however, of highly disordered staging for both donor- and acceptor-type GICs. For example, Huaw et al. reported the coexistence of several phases for single-crystal graphite intercalated with $CuCl_2$,[28] and Thomas et al. reported TEM images of disordered staging for a fine natural graphite powder intercalated with $FeCl_3$.[29] In some cases, stage disorder may well result from incomplete reaction kinetics, especially where the experiment involved the use of a highly crystalline graphite.

The disordered staging observed in these C_xPFOS products appears to derive from the limiting oxidative stability of the solvent rather than slow kinetics associated with rearrangement of large anions in these intercalated bilayers. This is supported by the formation of these same solid solution products within several hours at elevated temperature, as well as by the rapid formation of simple stage 2 GICs in mixed acids solutions described below.

Two energetic factors have been associated of the ordering of GICs into stages: the Coulombic repulsion of intercalated galleries and the elastic strain energy required to mechanically surround the intercalated domains by graphene layers. The unusual bilayer arrangement of anions, and associated large gallery height for C_xPFOS, will change the contribution of these terms significantly from that in most acceptor-type GICs. Despite the large volume of the $C_8F_{17}SO_3$ anion, the bilayer arrangement actually allows a relatively high charge density on the graphene layers, as can be gauged in low value of x considering the stage assignments. The correspondingly high positive charge density on the encasing graphene sheets will result in a repulsive term between graphene sheets that can be comparable to that in compounds such as C_xSO_3F, where $x \cong 7$ for stage 1.[30] The intercalant bilayers of $C_8F_{17}SO_3$ will likely mitigate Coulombic repulsion through the C_xPFOS

(25) Bell, R.; Bascombe, K.; McCoubrey, J. *J. Chem. Soc.* **1956**, 1286.
(26) Marcus, B.; Touzain, P. *Synth. Met.* **1988**, *23*, 13.
(27) Fuerst, C.; Fischer, J.; Axe, J.; Hastings, J.; McWhan, D. *Phys. Rev. Lett.* **1983**, *50*, 357.
(28) Hauw, C.; Gaultier, J.; Flandrois, S.; Gonzalez, O.; Dorignac, D.; Jagut, R. *Synth. Met.* **1983**, *7*, 313.
(29) Thomas, J.; Millward, G.; Schlogl, R.; Boehm, H. *Mater. Res. Bull.* **1980**, *15*, 671.
(30) Aubke, F.; Karunanithy, S. *J. Chim. Phys.* **1984**, *81*, 827.

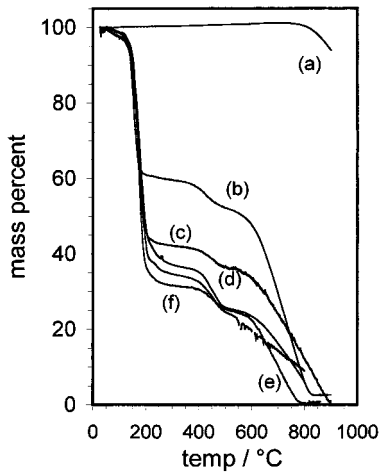

Figure 11. TGA curves (a) graphite, and C_xPFOS prepared in hydrofluoric acid after the following reaction times: (b) 1.5, (c) 3, (d) 24, (e) 72, and (f) 700 h.

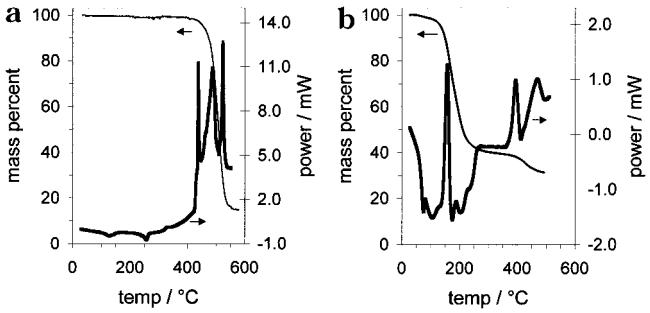

Figure 12. DSC and TGA curves for (a) KPFOS and (b) C_x-PFOS prepared in hydrofluoric acid (reaction time = 72 h).

galleries, but the predominant repulsive energy term that favors staging does not require a long-range interaction of that type. As for the mechanical elastic energies, it is difficult at this point to assess how these are affected, or even if the Daumas−Herold domain model can be employed with such large galleries.

Mass uptake, TGA, and elemental analyses on the products provide information on the product stoichiometries and identity of intercalating species. Four mass loss regions between 25 and 900 °C are seen in the TGA traces of GICs prepared in hydrofluoric acid. (Figure 11) The first loss, below 120 °C, ranges from 0.5 to 3 mass percent, with longer reaction times associated with a greater mass loss. The PXRD patterns do not significantly change after heating briefly in this temperature range, and the mass loss is ascribed to intercalated or surface-adsorbed H_2O or HF. The next two regions occur between 150−200 °C and 400−500 °C, with the former accounting for the majority of the mass loss. After heating at 300 °C, the GICs show only a broad reflection due to poorly crystalline graphite, so the ordered GIC structure has disappeared by this temperature. For comparison, $KC_8F_{17}SO_3$(s) shows a sharp mass decrease beginning at 420 °C. (Figure 12a) The remaining carbonaceous material is completely volatilized during the final mass loss beginning at 600 °C. This can be compared to graphite, which under these experimental conditions begins to lose mass at 650−800 °C. The presence of a small O_2 impurity in the N_2 purge gas is responsible for the combustion of graphitic carbon.

DSC analyses on KPFOS (Figure 12a) show a complex exothermic decomposition for the salt beginning at 420 °C. The C_xPFOS samples present several thermal events between ambient and 500 °C. The first is a broad endotherm between approximately 50 and 250 °C, within which occurs a large, relatively sharp, exothermic peak with onset at 130 °C. The endotherm is related to volatilization of species from the first two mass loss events noted above, and the sharp exotherm indicates a decomposition reaction of the GIC in mass loss region 2. The two exotherms observed between 400 and 500 °C are similar to those of KPFOS and suggest that mass loss in region 3 is related to $C_8F_{17}SO_3^-$ decomposition exterior to the graphite structure. This agrees with the loss of an ordered structure in samples annealed above 300 °C.

The mass uptake data are compared with the combined TGA mass losses below 500 °C in Table 2. The general similarity in mass uptake and loss indicates that these mass losses arise from the degradation of the anions to volatile species, without significant loss of graphene carbon. For this reason, the TGA loss data are taken as an approximate indicator of product stoichiometry, and the calculated mole ratios of graphene C to $C_8F_{17}SO_3^-$ are reported in the table. An exception occurs after long reaction time at 50 °C, where the precipitation of a manganese-containing byproduct leads to a significant overestimate by TGA of the intercalant content. Table 2 includes compositional data from elemental analyses that indicate significant excess of F relative to S in the compounds. There is an impurity of the fluorine-rich phases C_xF ($x \cong 3-4$), which accounts for part of the excess fluorine. Structural refinement (see below) also shows excess electron density in intercalated galleries ∼3−4 Å from each graphene carbon plane, which is ascribed to HF, fluoride, or bifluoride. In both analyses, the nominal compositions can be described as $C_xC_8F_{17}SO_3{\cdot}yF$, with y ranging from 3 to 5. The calculated values for x, the molar ratio of graphene C to $C_8F_{17}SO_3$, in Table 2, therefore assume $y = 4$.

The minimum value obtained for x is approximately 16−19, which agrees well with the value $x = 17$ obtained previously for the stage 2 compound prepared by electrochemical oxidation of graphite in CH_3NO_2.[12] The GICs obtained by this chemical route have galleries ∼3 Å smaller than those obtained by the electrochemical method, which suggests a significantly greater anion takeoff angle in the latter GICs. The principal compositional difference between these products is in the lack of excess fluoride in the electrochemical products, which appears to have a pronounced affect on the interaction of anions within the galleries.

The bilayer intercalant structure allows this relatively high intercalant content for the graphite galleries (∼1 anion/10 graphene carbons). On the basis of the relation between d_i and stage, the intercalant content, and volume (calculated at 344 Å^3 for $C_8F_{17}SO_3$), the gallery occupancies can be derived for different stage assignments. These are summarized in Table 3 for the pure stages and the solid solution model, and demonstrate that the assignment of the solid solution with second and third staging is in best agreement with the compositional data.

Products in Aqueous HF/HNO_3 and Aqueous HF/H_2SO_4. As noted above, the solvent oxidative stability can limit the extent of intercalation. Stage 1 GICs can

Table 2. Compositional Data from Mass Uptake, TGA, and Elemental Analyses for C_xPFOS Prepared in Hydrofluoric Acid or a Hydrofluoric Acid/Nitric Acid Cosolvent

HF/HNO_3, v/v[a]	*T*, °C	*t*, h	intercalant/C, g/g: by mass uptake	intercalant/C, g/g: by TGA	$C/C_8F_{17}SO_3$, mol/mol[b]	composition[c] by elem anal.
100/0	20	1.5	0.81	0.83	61.0	
100/0	20	3.0	1.46	1.45	33.0	
100/0	20	24	2.59	2.57	18.6	
100/0	20	72	2.82	2.56	18.7	$C_{28.2}C_8F_{17}SO_3{\cdot}4.8F$
100/0	20	700	3.17	2.94	16.3	
100/0	50	0.1	0.3	0.40	136	
100/0	50	0.3	1.42	1.87	25.6	
100/0	50	0.5	1.49	1.84	27.2	
100/0	50	1.5	2.14	2.45	19.6	
100/0	50	3.0	2.15	2.25	21.3	
100/0	50	24	2.83	2.89	16.6	
100/0	50	170	1.56	5.02	9.6	
17/83	20	24	2.25	2.70	17.7	$C_{22.2}C_8F_{17}SO_3{\cdot}4.0F$
33/66	20	24	2.63	2.66	18.0	
50/50	20	24	2.21	2.72	17.6	
87/13	20	24	2.16	1.86	25.8	

[a] Indicates relative vol % added of 48% HF and 69% HNO_3. [b] Calculated from TGA data as *x* in $C_xC_8F_{17}SO_3{\cdot}4F$. [c] Based on elemental analyses for C, S, N, and F.

Table 3. Occupied Volume Fraction of Expanded Galleries Calculated for Different Stage Assignments[a]

possible stage assignment: integral stage	possible stage assignment: mixed stage (0.70:0.30 relative content)	occupied volume fraction in gallery[b]
1		0.28
	1/2	0.40
2		0.66
	2/3	**0.80**
3		1.13
	3/4	1.26
4		1.52

[a] The fractional stage assignments reflect random solid solutions with probabilities of second staging:third staging::0.7:0.3. [b] The occupied volume fraction is calculated using a composition of $C_{18}C_8F_{17}SO_3{\cdot}4F$, d_i = 29.6 Å, vol ($C_8F_{17}SO_3$) = 344 Å^3, vol (F) = 16 Å^3.

Table 4. Fractional Stage Content Determined for C_xPFOS Prepared in Hydrofluoric Acid/Nitric Acid Cosolvents[a]

HF/HNO_3 v/v[b]	reaction time	fractional content: stage 1	stage 2	stage 3
83/17	24 h	0.03	0.97	
66/33	24 h		1.00	
50/50	24 h	0.05	0.95	
13/87	24 h		0.99	0.01
13/87	1 week		0.94	0.06

[a] In each case, the products can be fit well by a simple stage 2 model. [b] Indicates relative vol % added of 48% HF and 69% HNO_3.

be prepared in more highly concentrated acids, and a stage 1 C_xPFOS was prepared by electrochemical oxidation using organic solvents. For this reason, the addition of concentated nitric or sulfuric acid to hydrofluoric acid can allow a lower stage product to be obtained.

When we add K_2MnF_6 and $KC_8F_{17}SO_3$ to 69% HNO_3 (all other reaction conditions maintained as above), a reddish-brown color, presumed due to Mn(III), is observed immediately in solution, and slowly disappears over several hours to give a colorless solution and amorphous precipitate. The instability of K_2MnF_6 in 69% HNO_3 precludes the formation of a low-stage GIC in this solvent.[31] PXRD on the solid products obtained from reaction of graphite with the reddish-brown solution show stage 3 graphite nitrate and several broad, unassigned peaks. Heating this product to 900 °C generates crystalline Mn_3O_4.

The oxidant K_2MnF_6 is stable in nitric acid, however, when hydrofluoric acid is a cosolvent. Table 4 provides a summary of PXRD peak position analyses from reactions containing 13−83% (v/o) hydrofluoric acid in concentrated HNO_3. In each case, the pattern fits well as a simple stage 2 GIC, with minimal contribution (0−6%) due to other stages. A Williamson−Hall plot indicates a coherent domain length of 1200 Å, or ∼35 unit cell repeats, for the product obtained using 17% HF (Figure 7b). In addition to the formation of stage 2 GIC rather than the solid solution, the products obtained within this range of solvent compositions are obtained at shorter reaction time than those prepared in hydrofluoric acid. Hence, stage 2 GICs appear within 24 h at 20 °C.

Elemental analysis for N (<0.1%) in these products indicates that NO_3^- (or HNO_3) accounts for at most 4 mol % of intercalant species relative to the $C_8F_{17}SO_3$ anion. Since stage 2 or 3 graphite nitrate compounds are obtained within 30 min by this method when the $C_8F_{17}SO_3$ salt is not present, the larger anion either prevents intercalation of nitrate, or exchanges for the nitrate anion at longer reaction times. Compositions determined for the products obtained using the acid mixtures are very similar to those obtained in hydrofluoric acid (Table 2).

A similar phenomenon occurs by the addition of small amounts of H_2SO_4 to hydrofluoric acid. With a solvent composition of 17% (v/o) fuming H_2SO_4, a stage 2 C_x-PFOS is obtained within 24 h. If the sulfuric acid content is increased, however, the GIC product stage increases and a graphite sulfate phase is observed by PXRD. The stage 1 graphite sulfate compound ($I_c \cong 8.0$ Å) is the only product obtained with the H_2SO_4 content

(31) If a stable oxidant is used, $C_xC_8F_{17}SO_3$ can be obtained in 69% HNO_3. When graphite, excess PbO_2, and $KC_8F_{17}SO_3$ are added to hydrofluoric acid, the solid products contain stage 2 or 3 $C_xC_8F_{17}SO_3$, stage 2 graphite nitrate and PbO_2. Interestingly, the $C_xC_8F_{17}SO_3$ is stable in the acid as long as PbO_2(s) is present, but reverts back to graphite within 2 h in neat 69% HNO_3.

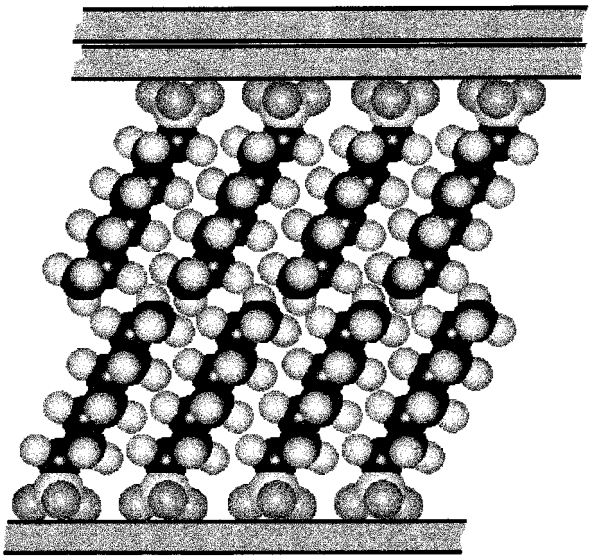

Figure 13. The bilayer intercalant arrangement in C_xPFOS.

above 50%. For reaction times greater than 24 h, even with the lower H_2SO_4 content, the C_xPFOS converts to graphite sulfate. Similarly, stirring a stage 2 C_xPFOS (obtained by other means) in fuming H_2SO_4 at ambient temperature results in its conversion to stage 1 graphite sulfate within 30 min.

These results are consistent with previous findings that GICs of singly charged anions are readily converted to graphite sulfate. For example, Avdeev et al., have described to exchange reaction to form graphite sulfate from graphite nitrate.[32] It is likely that the favorable lattice enthalpy associated with sulfate within the intercalant gallery provides the driving energy for this displacement.

Details on the intercalated gallery structure are obtained by refinement of the stage 2 product obtained using 17% HNO_3. As the anion length is ~15 Å, the gallery dimensions indicate that a bilayer intercalant structure is most reasonable.[9] The structural model employed places the three oxygens in each anionic $-SO_3$ headgroup in a plane parallel to graphite sheet, with hydrophobic fluorocarbon chains thus oriented toward the center of the gallery, as indicated in Figure 13. An initial takeoff angle, or angle between anionic chain and graphene carbon plane, of 54° is obtained from the S−C−C bond angle for the energy-minimized isolated anion. Subsequent refinement of the PXRD data provides a slightly greater takeoff angle of 57°. This requires the bilayers to nestle into one another by 2−3 Å at the gallery center.

A 1D electron density map generated from diffraction data is compared to that calculated from the structural model in Figure 14. The greatest electron density, at $z \cong 0.05$ (and 0.95), derives from the graphene carbon planes. The sulfonate groups contribute most of the electron density near $z = 0.15$ (and 0.85), but additional electron density is required to fit the PXRD data. As a simple model, a single plane of F density is included at ≅3−4 Å above the graphene layers, with the position of this plane found by refinement. The F stoichiometry

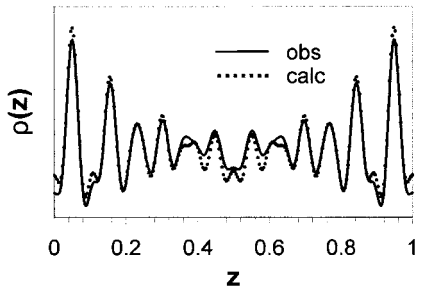

Figure 14. Electron density map derived from PXRD data and calculated for refined structural model of $C_{21.6}C_8F_{17}SO_3$·4F.

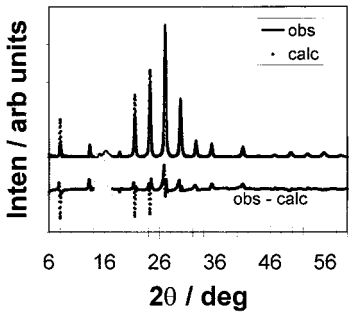

Figure 15. Observed and calculated PXRD patterns for C_x-PFOS prepared by 24-h reaction using 17% (v/o) HNO_3 in hydrofluoric acid. Data between 14 and 17.5° 2θ were excluded due to peaks ascribed to a C_xF impurity phase.

for the best fit lies in the range of $y = 3-5$ for $C_xC_8F_{17}$-SO_3·yF, and $y = 4$ is used for subsequent refinement. Peaks at $z = 0.22$, 0.30, 0.38, and 0.45 arise from successive $-CF_2-$ or $-CF_3$ units along the anionic chains, and these planes of electron density are used to refine both the takeoff angle and anion content in the galleries.

The electron density peak near $z = 0.38$ is notably broader than the others due to the inclusion of the branched isomer $(CF_3)_2C(F)C_5F_{10}SO_3^-$. This isomer contains two $-CF_3$ groups in the range $z \cong 0.38-0.41$. The isomeric content of the GIC may differ from that in the starting reagent due to selectivity during the intercalation process, and an improved fit to the data can be obtained by decreasing the linear isomer content below 70%. In the model employed, however, the linear isomer content is maintained at 70% and not further refined.

The four refined parameters and best fits obtained for the structural model are thus the chain takeoff angle (56.6 °), the graphene plane to sulfonate oxygen plane distance (3.04 Å), the graphene plane to fluoride plane distance (3.8 Å), and the graphene carbon/intercalant molar ratio ($x = 21.6$). These results provide a reliability factor $R = 0.082$ for $C_{21.6}C_8F_{17}SO_3$·4F. Figure 15 shows the observed and calculated PXRD for the product using this structural model.

The value for x obtained agrees reasonably well with those found from gravimetry ($x = 18$) and elemental analyses ($x = 22$) (Table 2). The graphene plane−O distance conforms to the anticipated result, in comparison this distance is 3.2 Å for graphite nitrate (stage 2, $I_c = 9.9$ Å). The graphene plane−F distance (3.8 Å), however, is somewhat larger than observed for other graphite compounds containing fluoride or bifluoride.

(32) Avdeev, V.; Sorokina, N.; Nikolskaya, I.; Monyakina, L.; Voronkina, A. *Inorg. Mater.* **1997**, *33*, 699.

Stage 1 planar-sheet graphite fluorides, C_xF, would have this distance at most in the range of 2.8−3.0 Å, assuming a central location of the fluoride in the galleries.[21] Due to the bilayer arrangement of fluoride in C_xF, and the semicovalent nature of the C−F interaction, much smaller values for this distance are likely in the graphite fluorides.[33,34] Stage 2 graphite bifluoride exhibits I_c = 9.83 Å, which can give a maximum graphene plane−F distance of 3.24 Å. In graphite bifluoride compounds, the location of bifluoride at the gallery center is far more likely due to the less covalent nature of the interaction. The larger distance observed for C_xPFOS suggests weaker interaction between the positive graphene carbon sheet and the fluoride-containing species. Since the model employed does not distinguish fluoride from bifluoride (or HF), and there is also the possibility of a distribution of distances in the product, further analysis of the interaction will require additional investigation.

Although a reasonable fit is obtained given the data set and number of refinement parameters employed, there are additional considerations that may significantly improve the structural model. Calculations indicate that energy-minimized perfluorocarbon chains are helical rather than linear, although the twist may be reduced when shorter chains are packed together.[35] The twist angle for these chains, and other parameters, such as the content of branched chain isomer in the GICs, are not refined due to the limited data set obtained using these conditions. Preliminary calculations, however, suggest that these additional parameters should be included in a more sophisticated structural model when a higher quality PXRD data set can be obtained.

Acknowledgment. The authors gratefully acknowledge support from NSF grant DMR-9419481. ^{19}F NMR data were obtained at Portland State University through Professor Gary Gard. The authors also thank Professor Gard and Professor Douglas Keszler at OSU for helpful discussions.

CM981060V

(33) Mallouk, T. Bartlett, N. *Phil. Trans. R. Soc. London* **1985**, *A314*, 179.

(34) Matsuo, Y.; Segawa, M.; Sugie, M. *J. Fluorine Chem.* **1998**, *87*, 145.

(35) Knochenhauer, G.; Reiche, J.; Brehmer, L.; Barberka, T.; Woolley, M.; Tredgold, R.; Hodge, P. *J. Chem. Soc., Chem. Commun.* **1995**, 1619.